Hindawi
International Journal of Aerospace Engineering
Volume 2022, Article ID 3256825, 19 pages
https://doi.org/10.1155/2022/3256825

Research Article

Thermal Analysis and Rigid-Flexible Coupling Dynamics of a Satellite with Membrane Antenna

Xiang Liu and Guoping Cai

Department of Engineering Mechanics, State Key Laboratory of Ocean Engineering, Shanghai Jiao Tong University, Shanghai 200240, China

Correspondence should be addressed to Guoping Cai; caigp@sjtu.edu.cn

Received 14 March 2022; Accepted 6 May 2022; Published 18 May 2022

Academic Editor: Zhiguang Song

In this paper, the thermal analysis of a membrane antenna structure is performed, and then, the rigid-flexible coupling dynamic modeling and control of the membrane-antenna-satellite system are studied with the thermal stress considered. The thermal analysis model of the membrane antenna structure is derived based on the finite element method by discretizing the structure into 1D and 2D thermal elements. Considering the thermal stress, the vibration modes of the membrane antenna structure are obtained, and the rigid-flexible coupling dynamic model of the membrane-antenna-satellite system is derived based on the hybrid coordinate method. To reduce the vibration of the membrane antenna structure caused by the attitude maneuver, the control command is designed based on the component synthesis vibration suppression (CSVS) method. Simulation results show that the dynamic properties of the membrane antenna structure are affected significantly by the space thermal environment, the vibration of the membrane antenna structure can be suppressed effectively by the presented CSVS controller, and the accuracy of the attitude maneuver will be improved significantly by the proposed control strategy.

1. Introduction

The large-scale space membrane antenna has attracted a lot of attention in recent years because of its great application prospect in the field of deep space exploration and space-based early warning and earth observation [1–4]. To maintain the in-orbit imaging quality of the membrane antenna, the surface accuracy and pointing accuracy must be conserved stringently [5, 6]; therefore, it is of great necessity to build a precise rigid-flexible coupling dynamic model and design an effective controller for the membrane-antenna-satellite system. For orbiting space structures, like the space membrane antenna, thermal deformation and thermal stress could be considerable because of the environmental and on-board heat sources [7–9]. For a membrane structure whose dynamic properties are dominated by the stress distribution [10, 11], thermal stress may change dynamics of the structure significantly. Therefore, it is of great theoretical significance and practical interest to study the rigid-flexible coupling dynamics and control of the membrane-antenna-satellite system considering thermal effects.

The rigid-flexible coupling dynamics and control of spacecraft with flexible appendages have been a research topic of continued interest in the past decades. Li and Yan [12] developed a numerical method for the thermal-structure model of a composite solar array to characterize the thermal-structure response of a rigid solar array in low Earth orbit. Liu et al. [13] studied the rigid-flexible-thermal coupling dynamics of spacecraft consisting of a rigid hub and a solar array. Liu and Pan [14] established a complete rigid-flexible-thermal coupling dynamic model for a low-Earth-orbit spacecraft composed of a satellite and solar array. Hu and Ma [15] proposed a novel approach integrating a component synthesis vibration suppression- (CSVS-) based command-shaping technique and positive position feedback (PPF) control to suppress the vibration of a flexible spacecraft actuated by on-off thrusters during attitude maneuvers. Hu et al. [16] studied the robust vibration

control of flexible spacecraft; a control strategy integrates the command input shaping and the technique of dynamic variable structure output feedback control is proposed. Liu et al. [17] studied the rigid-flexible coupling dynamic modeling and control of flexible spacecraft by using global analytical modes. Cao et al. [18] studied the rigid-flexible-thermal coupling dynamics of a spacecraft with lateral solar arrays in orbit; the thermal alternation-induced vibration is analyzed in this work. Based on the thermal integrated absolute nodal coordinate formulation, the rigid-flexible-thermal coupling dynamics of spacecraft carrying large-aperture paraboloid antenna is analyzed in Cui et al.'s work [19]. Shahravi and Azimi [20] studied the attitude and vibration control of flexible spacecraft by using a singular perturbation method; a nonlinear quaternion feedback control is chosen for the attitude control design and a strain rate feedback (SRF) scheme is developed for suppression of vibrational modes. Shahravi and Azimi [21] studied the vibration control of smart flexible substructures of satellite during attitude maneuver; a comparison between the collocated and noncollocated piezoceramic sensors/actuators is performed to investigate their effectiveness in suppressing vibration in flexible substructures. Azimi and Shahravi [22] proposed an adaptive variable structure control scheme employing a hybrid-sliding surface to treat the problems associated with the uncertainties, disturbances, and flexibility dynamic interactions of a spacecraft with large flexible sun-oriented solar panels. Azimi and Joubaneh [23] studied the dynamic modeling and vibration control of spacecraft with a flexible appendage embedded with piezoelectric patches; the strain rate feedback control law is utilized to suppress the vibration of the flexible appendage. Liu et al. [24] studied the dynamic responses and control strategy for a spacecraft with a large hoop-truss antenna under solar flux shock; the thermal flux is treated as an external excitation in this work, but the influence of thermal stress on the dynamic properties of the antenna structure is not considered. From the literature review, we can see that, in previous works, most investigations focused on spacecraft with regular-shaped flexible appendages, such as a beam, plate, or shell. However, the rigid-flexible coupling dynamics of spacecraft with irregular appendage, such as a membrane antenna structure, has been rarely studied. As for the dynamic studies of membrane antenna structures, some research works have been conducted in recent years. For example, Shen et al. [25] studied the vibration mode shapes and natural frequencies of a synthetic aperture radar (SAR) membrane antenna under different pretensions. Fang et al. [26] analyzed the vibration of an eight-meter-diameter membrane reflect-array antenna using the two-variable-parameter (2-VP) method combined with the distributed transfer function method (DTFM). Liu et al. [27, 28] studied the dynamic modeling and active vibration control of a tensioned membrane antenna structure with piezoelectric actuators and cable actuators. All these works focused on the structural dynamic problems of the membrane antenna structure, whereas the rigid-flexible coupling dynamics of a satellite with membrane antenna has rarely been investigated. Very recently, Liu et al. [6] studied the rigid-flexible coupling dynamic modeling and hybrid control of a satellite with membrane antenna; however, the thermal effects which may affect the dynamics of the membrane structure significantly are not considered.

This paper is a follow-up research of our previous work [6]. The major contributions of this work are the rigid-flexible coupling dynamic modeling and vibration control of membrane antenna spacecraft considering thermal effects. The thermal analysis of the membrane antenna structure is performed under actual orbit and satellite attitude first; then, considering the influence of thermal stress on dynamic properties of the membrane antenna structure, the rigid-flexible coupling dynamic model of the spacecraft is established, and a controller is designed to suppress the vibration of the membrane antenna structure caused by attitude maneuver. The remainder of this paper is organized as follows. In Section 2, the thermal model of the membrane antenna structure is established based on the finite element method (FEM). Then, in Section 3, considering the thermal effects, the rigid-flexible coupling dynamic model of the membrane-antenna-satellite system is derived by using the hybrid coordinate method, and a controller is designed based on the component synthesis vibration suppression method. Numerical simulation results are presented in Section 4. Finally, in Section 5, major conclusion remarks are summarized.

2. Thermal Analysis of the Membrane Antenna Structure

The membrane-antenna-satellite system studied in this paper is shown in Figure 1, which contains two major parts, i.e., the satellite and the membrane antenna structure. The deformation of the satellite is negligible; therefore, the satellite is termed as a rigid hub, and the membrane antenna structure is termed as a flexible appendage in our study. The membrane antenna structure is fixed to the satellite through four rigid connecting poles whose masses are neglected. Since the satellite is termed as a rigid hub, the thermal deformation of the satellite is neglected. The membrane antenna structure consists of five main components: membrane array, support frame, tensioning mechanism, lap device, and tension pole, as shown in Figure 1.

The Sun and Earth are the primary heat sources for spacecraft in Earth orbit [29, 30]. For the membrane antenna structure studied in this paper, the external thermal load mainly includes direct solar radiation q_s, Earth-emitted radiation q_e, and Earth-reflected radiation (albedo) q_a, as shown in Figure 2. The heat flux on a structural member depends on the orbit altitude and the member's orientation with respect to the Sun and Earth. In our study, Earth shadowing is considered in the thermal analysis. Once the spacecraft enters the Earth's shadow, there will be no direct solar radiation and Earth albedo [31].

As shown in Figure 1, for the membrane antenna structure, in the thermal analysis, the support frame is modeled with a 1D thermal element, and the membrane array is modeled with a 2D thermal element. For simplicity and because of the low thermal conductivity of the cables, the tensioning

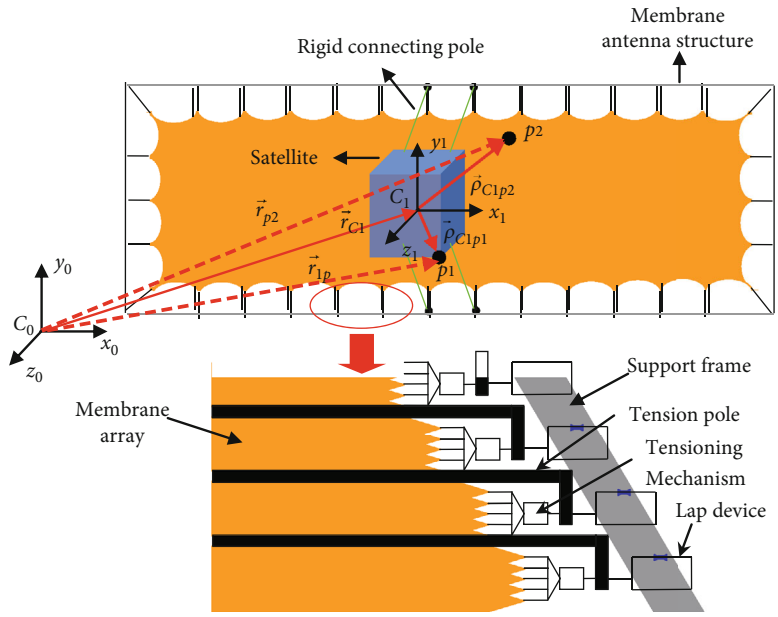

Figure 1: Satellite with membrane antenna structure.

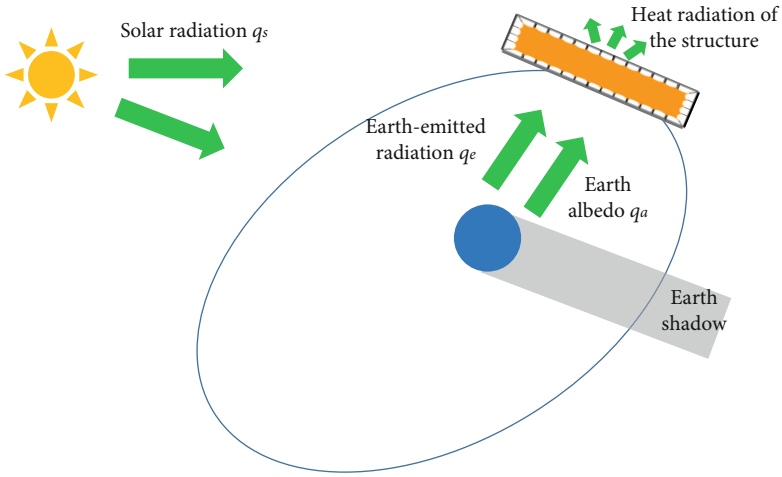

Figure 2: Thermal environment in Earth orbit.

mechanism, lap device, and tension pole are neglected in the thermal analysis. Since the space environment is nearly vacuum, heat convection is not considered in the thermal analysis. Based on the heat conduction and radiation relationships, the thermal balance equations can be established, and then, the thermal models of the 1D and 2D elements are obtained. The modeling of the 1D and 2D thermal elements is presented as follows.

2.1. 1D Thermal Element Modeling. As shown in Figure 3, a two-node 1D thermal element is used to discretize the support frame in our work. Based on the thermal balance equation, the temperature field $T(x,t)$ in the 1D thermal element is governed by [32]

$$\lambda A\frac{\partial^2 T}{\partial x^2} - P\varepsilon\sigma T^4 + (q_s + q_e + q_a)D = A\rho c\frac{\partial T}{\partial t}, \quad (1)$$

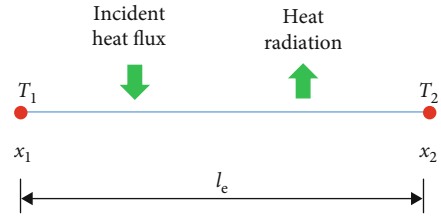

Figure 3: Two-node 1D thermal element.

where the first term on the left side represents the thermal conduction in the 1D thermal element, the second term on the left side represents the thermal radiation of the 1D thermal element, the third term on the left side represents the external thermal load, the term on the

right side represents the temperature change of the 1D thermal element, λ is the thermal conductivity, A is the cross-section area of the 1D element, P is the perimeter of the cross-section area of the 1D element, ε represents the emissivity, D is the diameter of the 1D element, ρ represents the density of the 1D element, and c is the heat capacity.

Based on equation (1), the temperature functional for the 1D thermal element can be expressed as

$$I^e = \int_{x_1}^{x_2} \left[\frac{1}{2}\lambda A \left(\frac{\partial T}{\partial x} \right)^2 + \frac{1}{5} P\varepsilon\sigma T^5 - (q_s + q_e + q_a)DT + A\rho c \frac{\partial T}{\partial t} T \right] dx. \tag{2}$$

By using the FEM [33], the temperature field in the 1D thermal element can be written as

$$T(x,t) = N_1(x)T_1(t) + N_2(x)T_2(t), \tag{3}$$

where T_1 and T_2 represent the nodal temperature and $N_1(x)$ and $N_2(x)$ are the interpolation functions, whose expressions are

$$N_1(x) = \frac{x_2 - x}{l_e}, \tag{4a}$$

$$N_2(x) = \frac{x - x_1}{l_e}. \tag{4b}$$

Here, $l_e = x_2 - x_1$ represents the length of the element.

Substituting equation (3) into equation (2), and calculating the variation of the functional I^e, the thermal equation for the 1D element in the finite element form can be derived as

$$\begin{aligned} 0 = \begin{bmatrix} \dfrac{\partial I^e}{\partial T_1} \\ \dfrac{\partial I^e}{\partial T_2} \end{bmatrix} = f^e &= \frac{\lambda A}{l_e} \begin{bmatrix} T_1 - T_2 \\ T_2 - T_1 \end{bmatrix} + \frac{2}{3} P\varepsilon l_e \sigma T_r^3 \begin{bmatrix} 2T_1 + T_2 \\ T_1 + 2T_2 \end{bmatrix} \\ &- \frac{3}{2} P\varepsilon l_e \sigma T_r^4 \begin{bmatrix} 1 \\ 1 \end{bmatrix} - \frac{1}{2} l_e D(q_s + q_e + q_a) \begin{bmatrix} 1 \\ 1 \end{bmatrix} + \frac{A\rho c l_e}{6} \\ &\cdot \begin{bmatrix} 2\dfrac{\partial T_1}{\partial t} + \dfrac{\partial T_2}{\partial t} \\ \dfrac{\partial T_1}{\partial t} + 2\dfrac{\partial T_2}{\partial t} \end{bmatrix}, \end{aligned} \tag{5}$$

in which the approximate linearization of the 4-th order term, $T^4 = 4T_r^3 T - 3T_r^4$, is used [34]; here, $T_r = (T_1 + T_2)/2$.

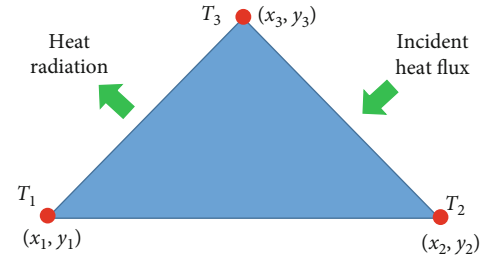

Figure 4: Three-node 2D triangle thermal element.

By using the numerical differentiation method, $\partial T_i/\partial t$ can be expressed as $\partial T_i/\partial t = (T_1^t - T_1^{t-1})/\Delta t$, $i = 1, 2$; then, equation (5) can be rewritten as

$$\begin{aligned} &\frac{\lambda A}{l_e} \begin{bmatrix} T_1^t - T_2^t \\ T_2^t - T_1^t \end{bmatrix} + \frac{1}{12} P\varepsilon l_e \sigma \left(T_1^t + T_2^t \right)^3 \begin{bmatrix} 2T_1^t + T_2^t \\ T_1^t + 2T_2^t \end{bmatrix} \\ &- \frac{3}{32} P\varepsilon l_e \sigma \left(T_1^t + T_2^t \right)^4 \begin{bmatrix} 1 \\ 1 \end{bmatrix} - \frac{1}{2} l_e D(q_s + q_e + q_a) \begin{bmatrix} 1 \\ 1 \end{bmatrix} \\ &+ \frac{A\rho c l_e}{6\Delta t} \begin{bmatrix} 2T_1^t + T_2^t \\ T_1^t + 2T_2^t \end{bmatrix} - \frac{A\rho c l_e}{6\Delta t} \begin{bmatrix} 2T_1^{t-1} + T_2^{t-1} \\ T_1^{t-1} + 2T_2^{t-1} \end{bmatrix} = 0, \end{aligned} \tag{6}$$

where T_i^t represents the nodal temperature of the 1D thermal element on the current time step, $i = 1, 2$; T_i^{t-1} represents the temperature on the last time step; and Δt represents the step size. Based on equation (6), the transient temperature in the 1D thermal element can be calculated step by step.

2.2. 2D Thermal Element Modeling. A three-node 2D triangle thermal element has been used to discretize the membrane array in our work, as shown in Figure 4. Like the 1D thermal element, according to the Fourier heat conduction law, the differential equation of the temperature field $T(x, y, t)$ in the 2D element can be expressed as [32]

$$h\left(\lambda_x \frac{\partial^2 T}{\partial x^2} + \lambda_y \frac{\partial^2 T}{\partial y^2} \right) - 2\varepsilon\sigma T^4 + (q_s + q_a + q_e) = h\rho c \frac{\partial T}{\partial t}, \tag{7}$$

where the first term on the left side represents the thermal conduction in the 2D thermal element, the second term on the left side represents the thermal radiation of the 2D thermal element, the third term on the left side represents the external thermal load, the term on the right side represents the temperature changing of the 2D thermal element, h represents the thickness of the 2D element, and λ_x and λ_y are the thermal conductivity in the x direction and y direction, respectively.

Based on equation (7), the temperature functional for the 2D thermal element can be obtained as

$$I^e = h\iint_{A_e}\frac{1}{2}\left[\lambda_x\left(\frac{\partial T}{\partial x}\right)^2+\lambda_y\left(\frac{\partial T}{\partial y}\right)^2\right]dxdy+\iint_{A_e}\frac{2}{5}\varepsilon\sigma T^5dxdy - \iint_{A_e}(q_s+q_a+q_e)Tdxdy+h\iint_{A_e}\rho c\frac{\partial T}{\partial t}Tdxdy, \tag{8}$$

where A_e represents the area of the 2D element.

By using the FEM, the temperature field in the 2D thermal element can be written as

$$T(x,y,t)=N_1(x,y)T_1(t)+N_2(x,y)T_2(t)+N_3(x,y)T_3(t), \tag{9}$$

where T_1, T_2, and T_3 represent the nodal temperature and $N_1(x,y)$, $N_2(x,y)$, and $N_3(x,y)$ are the interpolation functions, whose expressions are [33]

$$N_1(x,y)=\frac{1}{2A_e}[(x_2y_3-x_3y_2)+(y_2-y_3)x+(x_3-x_2)y], \tag{10a}$$

$$N_2(x,y)=\frac{1}{2A_e}[(x_3y_1-x_1y_3)+(y_3-y_1)x+(x_1-x_3)y], \tag{10b}$$

$$N_3(x,y)=\frac{1}{2A_e}[(x_1y_2-x_2y_1)+(y_1-y_2)x+(x_2-x_1)y], \tag{10c}$$

where A_e represents the area of the triangle thermal element.

Let $b_1=y_2-y_3$, $b_2=y_3-y_1$, $b_3=y_1-y_2$, $c_1=x_3-x_2$, $c_2=x_1-x_3$, $c_3=x_2-x_1$, and then, substituting equation (9) into equation (8), the thermal equation for the 2D element in the finite element form can be derived as

$$0=\begin{bmatrix}\frac{\partial I^e}{\partial T_1}\\ \frac{\partial I^e}{\partial T_2}\\ \frac{\partial I^e}{\partial T_3}\end{bmatrix}=f^e=\frac{h\lambda_x}{4A_e}\begin{bmatrix}b_1^2T_1+b_1b_2T_2+b_1b_3T_3\\ b_2b_1T_1+b_2^2T_2+b_2b_3T_3\\ b_3b_1T_1+b_3b_2T_2+b_3^2T_3\end{bmatrix}+\frac{h\lambda_y}{4A_e}\cdot\begin{bmatrix}c_1^2T_1+c_1c_2T_2+c_1c_3T_3\\ c_2c_1T_1+c_2^2T_2+c_2c_3T_3\\ c_3c_1T_1+c_3c_2T_2+c_3^2T_3\end{bmatrix}+\frac{2\varepsilon\sigma A_e}{81}(T_1+T_2+T_3)^3\begin{bmatrix}T_1\\ T_2\\ T_3\end{bmatrix} - \frac{A_e}{3}\alpha(q_s+q_a+q_e)\begin{bmatrix}1\\ 1\\ 1\end{bmatrix}+\frac{h\rho cA_e}{12}\cdot\begin{bmatrix}2\frac{\partial T_1}{\partial t}+\frac{\partial T_2}{\partial t}+\frac{\partial T_3}{\partial t}\\ \frac{\partial T_1}{\partial t}+2\frac{\partial T_2}{\partial t}+\frac{\partial T_3}{\partial t}\\ \frac{\partial T_1}{\partial t}+\frac{\partial T_2}{\partial t}+2\frac{\partial T_3}{\partial t}\end{bmatrix} \tag{11}$$

By using the numerical differentiation method, $\partial T_i/\partial t$ can be expressed as $\partial T_i/\partial t=(T_1^t-T_1^{t-1})/\Delta t$, $i=1,2,3$; then, equation (11) can be rewritten as

$$\frac{h\lambda_x\left(b_1T_1^t+b_2T_2^t+b_3T_3^t\right)}{4A_e}\begin{bmatrix}b_1\\ b_2\\ b_3\end{bmatrix}+\frac{h\lambda_y\left(c_1T_1^t+c_2T_2^t+c_3T_3^t\right)}{4A_e}\cdot\begin{bmatrix}c_1\\ c_2\\ c_3\end{bmatrix}+\frac{2\varepsilon\sigma A_e}{81}\left(T_1^t+T_2^t+T_3^t\right)^3\begin{bmatrix}T_1^t\\ T_2^t\\ T_3^t\end{bmatrix}-\frac{A_e}{3}\alpha(q_s+q_a+q_e)\begin{bmatrix}1\\ 1\\ 1\end{bmatrix}+\frac{h\rho cA_e}{12\Delta t}\begin{bmatrix}2T_1^t+T_2^t+T_3^t\\ T_1^t+2T_2^t+T_3^t\\ T_1^t+T_2^t+2T_3^t\end{bmatrix}-\frac{h\rho cA_e}{12\Delta t}\begin{bmatrix}2T_1^{t-1}+T_2^{t-1}+T_3^{t-1}\\ T_1^{t-1}+2T_2^{t-1}+T_3^{t-1}\\ T_1^{t-1}+T_2^{t-1}+2T_3^{t-1}\end{bmatrix}=0, \tag{12}$$

where T_i^t represents the nodal temperature of the 2D thermal element on the current time step, $i=1,2,3$; T_i^{t-1} represents the temperature on the last time step; and Δt represents the step size. Based on equation (12), the transient temperature in the 2D thermal element can also be calculated step by step.

2.3. Thermal-Elastic Model of the Membrane Antenna Structure. Based on equations (5) and (11), the finite element thermal equation for the whole structure can be obtained by assembling the thermal model of each element properly, which can be expressed as

$$f(T)=0, \tag{13}$$

where T represents the nodal temperature of the whole structure.

Equation (13) is a nonlinear algebraic equation about the temperature field in the structure, which can be solved by using the Newton iteration method, given by

$$T^{i+1}=T^i-\bar{f}^{-1}f, \tag{14}$$

where T^i represents the nodal temperature at the current iteration step, T^{i+1} represents the nodal temperature on the next iteration step, and $\bar{f}=df/dT$.

Once the temperature field of the structure is obtained based on equation (13), the thermal strain of the 1D and 2D thermal elements can be calculated. For the mechanical model of the membrane antenna structure, the support frame is modeled with two-node beam elements and the membrane array is modeled with three-node triangle membrane elements. The expressions of the thermal strain in the 1D (beam) element and 2D (membrane) element are

$$\xi_{1D}^T=[\alpha\Delta T_{1D},0,0,0,0,0]^T,\quad \xi_{2D}^T=[\alpha\Delta T_{2D},\alpha\Delta T_{2D},0]^T, \tag{15}$$

where α represents the thermal expansion coefficient; $\Delta T_{1D} = (T_{1D}^1 + T_{1D}^2)/2 - T_{1D}^{\text{ref}}$ (here, T_{1D}^{ref} represents the reference temperature of the 1D element and T_{1D}^1 and T_{1D}^2 represent the nodal temperature of the 1D element); and $\Delta T_{2D} = (T_{2D}^1 + T_{2D}^2 + T_{2D}^3)/3 - T_{2D}^{\text{ref}}$ (here, T_{2D}^{ref} represents the reference temperature of the 2D element and T_{2D}^1, T_{2D}^2, and T_{2D}^3 represent the nodal temperature of the 2D element).

And then, the thermal stress of the 1D (beam) element and 2D (membrane) element can be obtained as

$$\sigma_{1D} = D_{1D}B_{1D}\delta_{1D} - D_{1D}\xi_{1D}^T + \sigma_{1D}^0, \tag{16a}$$

$$\sigma_{2D} = D_{2D}B_{2D}\delta_{2D} - D_{2D}\xi_{2D}^T + \sigma_{2D}^0, \tag{16b}$$

where D_{1D} and D_{2D} represent the elastic matrixes for the 1D beam element and 2D membrane element, respectively; B_{1D} and B_{2D} represent the geometric matrixes for the 1D beam element and 2D membrane element, respectively; δ_{1D} and δ_{2D} represent the displacement vectors for the 1D beam element and 2D membrane element, respectively; σ_{1D}^0 and σ_{2D}^0 represent the prestress vectors for the 1D beam element and 2D membrane element, respectively.

3. Dynamic Modeling and Control of the Satellite with Membrane Antenna considering Thermal Stress

3.1. Rigid-Flexible Coupling Dynamic Modeling. Based on the thermal analysis results, the dynamic equation of the membrane antenna structure can be established by using FEM. The details have been presented in our previous work [27], which are not repeated here. The dynamic equation for the membrane antenna structure considering thermal stress can be expressed as

$$M\ddot{X} + C\dot{X} + \left(K + K^T\right)X = 0, \tag{17}$$

where X is the generalized coordinates of the structure, which only contains nodal displacements; M is the global mass matrix; K is the global stiffness matrix without considering thermal effect; K^T is the global stiffness matrix caused by thermal stress which can be calculated by using FEM based on the thermal stress in each element (the heat flux imposed on the membrane structure will change with attitude maneuvering; therefore,$K^T$is related to the attitude during the rigid-flexible coupling dynamic modeling); and C is the global damping matrix. In our work, the Rayleigh damping model $C = \alpha M + \beta K$ is adopted; here, α and β are the Rayleigh damping coefficients. Consulting Shen et al.'s work [25], the values of α and β are set as $\alpha = 0.01$ and $\beta = 0.01$ in this paper.

By using the modal truncation method, we can have

$$X(t) = \bar{\Phi}(t)\eta(t), \tag{18}$$

where $\bar{\Phi}(t)$ is the modal matrix obtained by equation (17) (because the stiffness matrix of the system is related to the attitude; therefore, $\bar{\Phi}(t)$ is time-variant during attitude maneuver); $\eta(t)$ represents the modal coordinates.

Let $\bar{\Phi}(t) = \Phi B(t)$; Φ is a time-invariant modal matrix, and $B(t)$ is the expansion coefficient matrix which represents the time-variant properties of $\bar{\Phi}(t)$ [35]; then, equation (18) can be rewritten as

$$X(t) = \Phi B(t)\eta(t) = \Phi a(t), \tag{19}$$

where $a(t)$ represents the generalized modal coordinates of the structure.

Substituting equation (19) into equation (17), and premultiplying the equation with Φ^T, it can be derived that

$$M_a\ddot{a} + C_a\dot{a} + K_a a = 0, \tag{20}$$

where $M_a = \Phi^T M \Phi$ is the modal mass matrix, $C_a = \Phi^T C \Phi$ is the modal damping matrix, and $K_a = \Phi^T(K + K^T)\Phi$ is the modal stiffness matrix.

As shown in Figure 1, define $C_0x_0y_0z_0$ as the inertial reference frame and $C_1x_1y_1z_1$ as the reference frame fixed on the satellite; C_1 is the centroid of the satellite. For point p_1 (which is on the satellite) and point p_2 (which is on the membrane antenna structure), we can have that

$$\vec{\mathbf{r}}_{p1} = \vec{\mathbf{r}}_{C1} + \vec{\boldsymbol{\rho}}_{C1p1}, \tag{21}$$

$$\vec{\mathbf{r}}_{p2} = \vec{\mathbf{r}}_{C1} + \vec{\boldsymbol{\rho}}_{C1p2}, \tag{22}$$

where $\vec{r}_{C1}$ represents the displacement of C_1; $\vec{\rho}_{C1p1}$ represents the relative displacement of p_1 to C_1; and $\vec{\boldsymbol{\rho}}_{C1p2} = \vec{\boldsymbol{\rho}}_{C1p2}^0 + \vec{\mathbf{u}}_{p2}$ represents the relative displacement of p_2 to C_1 (here, $\vec{\rho}_{C1p2}^0$ represents the relative displacement of transport point of p_2 to C_1 and $\vec{u}_{p2}$ represents the flexible deformation at p_2). $\vec{u}_{p2}$ can be expressed into matrix form as

$$u_{p2} = \Phi a. \tag{23}$$

Based on equations (21) and (22), it can be derived that

$$\dot{\vec{\mathbf{r}}}_{p1} = \dot{\vec{\mathbf{r}}}_{C1} + \vec{\boldsymbol{\omega}} \times \vec{\boldsymbol{\rho}}_{C1p1}, \tag{24}$$

$$\dot{\vec{\mathbf{r}}}_{p2} = \dot{\vec{\mathbf{r}}}_{C1} + \vec{\boldsymbol{\omega}} \times \vec{\boldsymbol{\rho}}_{C1p2} + \vec{\mathbf{v}}_{p2}, \tag{25}$$

where $\vec{\omega}$ is the rotational angular velocity of the satellite (because the satellite and membrane antenna are fixed through the rigid connecting poles, the angular velocity of the membrane antenna will also be $\vec{\omega}$) and $\vec{v}_{p2}$ represents the relative velocity of p_2 to C_1 introduced by the flexible deformation; the expression of $\vec{v}_{p2}$ is

$$\vec{v}_{p2} = \mathring{\vec{u}}_{p2}, \tag{26}$$

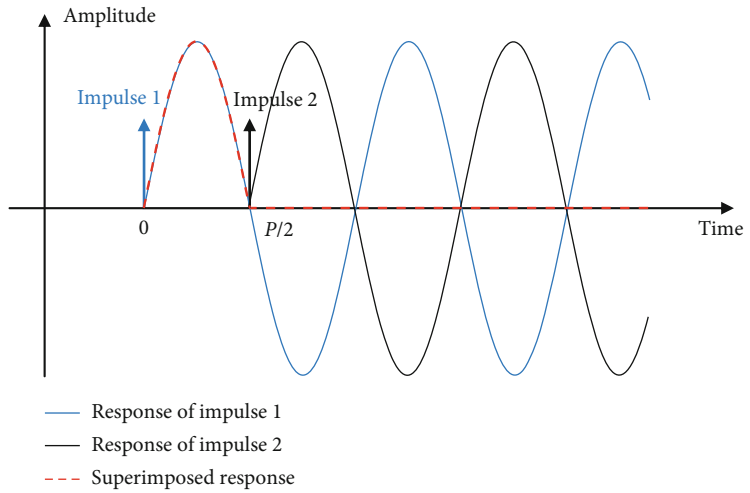

Figure 5: Basic principle of CSVS.

where $\vec{u}^{\circ}_{p2}$ represents the differentiation of vector $\vec{u}_{p2}$ in the $C_1x_1y_1z_1$ frame. $\vec{v}_{p2}$ can be expressed into matrix form as $v_{p2} = \Phi\dot{a}$.

Based on equations (24)–(26), the kinetic energy of the membrane-antenna-satellite system can be expressed as

$$E = E_1 + E_2, \tag{27}$$

where E_1 is the kinetic energy of the satellite and E_2 is the kinetic energy of the membrane antenna structure. The expressions of E_1 and E_2 are

$$\begin{aligned} E_1 &= \sum \frac{1}{2} m_{p1} \dot{\vec{\mathbf{r}}}_{C1} \cdot \dot{\vec{\mathbf{r}}}_{C1} + \sum m_{p1} \dot{\vec{\mathbf{r}}}_{C1} \cdot \left(\vec{\boldsymbol{\omega}} \times \vec{\boldsymbol{\rho}}_{C1p1}\right) \\ &\quad + \sum \frac{1}{2} m_{p1} \left(\vec{\boldsymbol{\omega}} \times \vec{\boldsymbol{\rho}}_{C1p1}\right) \cdot \left(\vec{\boldsymbol{\omega}} \times \vec{\boldsymbol{\rho}}_{C1p1}\right) \\ &= \sum \frac{1}{2} m_{p1} \dot{\vec{\mathbf{r}}}_{C1} \cdot \dot{\vec{\mathbf{r}}}_{C1} + \sum \frac{1}{2} m_{p1} \left(\vec{\boldsymbol{\omega}} \times \vec{\boldsymbol{\rho}}_{C1p1}\right) \cdot \left(\vec{\boldsymbol{\omega}} \times \vec{\boldsymbol{\rho}}_{C1p1}\right), \\ E_2 &= \sum \frac{1}{2} m_{p2} \dot{\vec{\mathbf{r}}}_{C1} \cdot \dot{\vec{\mathbf{r}}}_{C1} + \sum \frac{1}{2} m_{p2} \left(\vec{\boldsymbol{\omega}} \times \vec{\boldsymbol{\rho}}_{C1p2}\right) \cdot \left(\vec{\boldsymbol{\omega}} \times \vec{\boldsymbol{\rho}}_{C1p2}\right) \\ &\quad + \sum \frac{1}{2} m_{p2} \vec{\mathbf{v}}_{p2} \cdot \vec{\mathbf{v}}_{p2} + \sum m_{p1} \dot{\vec{\mathbf{r}}}_{C1} \cdot \left(\vec{\boldsymbol{\omega}} \times \vec{\boldsymbol{\rho}}_{C1p2}\right) \\ &\quad + \sum m_{p1} \dot{\vec{\mathbf{r}}}_{C1} \cdot \vec{\mathbf{v}}_{p2} + \sum m_{p1} \vec{\mathbf{v}}_{p2} \cdot \left(\vec{\boldsymbol{\omega}} \times \vec{\boldsymbol{\rho}}_{C1p2}\right), \end{aligned} \tag{28}$$

where m_{p1} represents the mass of point p_1 and m_{p2} represents the mass of point p_2.

Neglecting the influence of gravity, the potential energy of the membrane-antenna-satellite system can be expressed as

$$U = \frac{1}{2} a^T K_a a. \tag{29}$$

By using Lagrange's equation, the dynamic equation of the membrane-antenna-satellite system can be derived into matrix form as

$$\begin{aligned} \frac{d}{dt}\left(\frac{\partial E}{\partial r_{C1}}\right) = F_{C1} &= (m_1 + m_2)\ddot{r}_{C1} - A\sum m_{p2} \widetilde{\rho'}_{C1p2} A^T \dot{\omega} \\ &\quad + A\sum m_{p2} \Phi' \ddot{a} + \tilde{\omega}\tilde{\omega} A \sum m_{p2} \rho'_{C1p2} \\ &\quad + 2\tilde{\omega} A \sum m_{p2} \Phi' \dot{a}, \end{aligned}$$

$$\begin{aligned} \frac{d}{dt}\left(\frac{\partial E}{\partial \omega}\right) = M_{C1} &= A\sum m_{p2} \tilde{\rho}'_{C1p2} A^T \ddot{r}_{C1} + A\left(J'^1_{C1} + J'^2_{C1}\right) A^T \dot{\omega} \\ &\quad + A\sum m_{p2} \tilde{\rho}'_{C1p2} \Phi' \ddot{a} + \tilde{\omega} A \sum m_{p2} \tilde{\rho}'_{C1p2} A^T \dot{r}_{C1} \\ &\quad - \dot{\tilde{r}}_{C1} A \sum m_{p2} \Phi' \dot{a} + \tilde{\omega} A \left(J'^1_{C1} + J'^2_{C1}\right) A^T \omega \\ &\quad + 2A \sum m_{p2} \tilde{\rho}'_{C1p2} A^T \tilde{\omega} A \Phi' \dot{a}, \end{aligned}$$

$$\begin{aligned} \frac{d}{dt}\left(\frac{\partial E}{\partial \dot{a}}\right) + \frac{\partial U}{\partial a} = F_a - F_{\text{Damp}} &= \sum m_{p2} \Phi'^T A^T \ddot{r}_{C1} + \sum m_{p2} \\ &\quad \cdot \left(A \tilde{\rho}'_{C1p2} \Phi'\right)^T \dot{\omega} + \sum m_{p2} \Phi'^T \Phi' \ddot{a} \\ &\quad + 2\sum m_{p2} \Phi'^T A^T \tilde{\omega} A \Phi' \dot{a} \\ &\quad + \sum m_{p2} \Phi^T A^T \tilde{\omega}\tilde{\omega} A \tilde{\rho}'_{C1p2} + K_a a, \end{aligned} \tag{30}$$

where F_{C1} represents the external force at C_1; M_{C1} represents the external moment at C_1; F_a represents the external force applied on the membrane antenna in the modal coordinate; and F_{Damp} represents the damping force of the membrane antenna structure, $F_{\text{Damp}} = C_a \dot{a}$ (here, C_a is the modal damping matrix of the membrane antenna structure, $C_a = \alpha M_a + \beta K_a$). For arbitrary vector $\vec{z}$, $z = [z_1, z_2, z_3]^T$ represents the

Table 1: Mechanical and thermal parameters of the membrane-antenna-satellite system.

Components	Material property	Value
Satellite	Length (m)	1
	Width (m)	1
	Height (m)	1
	Mass (kg)	150
	Rotational inertia J_{11} (kg_*m^2)	25
	Rotational inertia J_{22} (kg_*m^2)	25
	Rotational inertia J_{33} (kg_*m^2)	25
Membrane antenna-membrane array	Young's modulus (GPa)	2.5
	Poisson's ratio	0.34
	Density (kg/m^3)	1530
	Length (m)	23.4
	Width (m)	5.6
	Thickness (m)	0.00025
	Heat capacity (J/kg_*K)	1000
	Thermal conductivity in the x direction (W/m_*K)	0.12
	Thermal conductivity in the y direction (W/m_*K)	0.12
	Thermal expansion (1/K)	0.00001
	Absorptivity	0.8
	Emissivity	0.8
	Reference temperature (K)	295
Membrane antenna-support frame	Young's modulus (GPa)	40
	Poisson's ratio	0.3
	Density (kg/m^3)	1800
	Length (m)	24
	Width (m)	7
	Cross-section area of the beam in the x direction (m^2)	0.000318
	Moment of inertia of z-axis for the beam in the x direction (m^4)	0.00000126
	Moment of inertia of y-axis for the beam in the x direction (m^4)	0.00000037
	Cross-section area of the beam in the y direction (m^2)	0.000877
	Moment of inertia of z-axis for the beam in the y direction (m^4)	0.00000112
	Moment of inertia of y-axis for the beam in the y direction (m^4)	0.00000132
	Heat capacity (J/kg_*K)	1000
	Thermal conductivity (W/m_*K)	32.11
	Thermal expansion (1/K)	0.00001
	Absorptivity	0.8
	Emissivity	0.8
	Reference temperature (K)	295
Membrane antenna-tension cable	Young's modulus (GPa)	133
	Poisson's ratio	0.36
	Density (kg/m^3)	1440
	Cross-section area (m^2)	0.000000049
	Tension of cable along x-axis (N)	51.2
	Tension of cable along y-axis (N)	54
	Tension of diagonal cable (N)	75.4

Table 1: Continued.

Components	Material property	Value
Membrane antenna-tension pole	Young's modulus (GPa)	210
	Poisson's ratio	0.3
	Density (kg/m^3)	1800
	Length (m)	7
	Cross-section area (m^2)	0.000178
	Moment of inertia of z-axis (m^4)	0.0000000125
	Moment of inertia of y-axis (m^4)	0.0000000125

Table 2: Orbital parameters for the membrane antenna.

	Semimajor axis (km)	Eccentricity	Inclination (°)	Longitude of the ascending node (°)	Argument of perigee (°)	Orbital period (h)
Low orbit	8869	0.3798	30	45	0	2.31
High orbit	72545	0.2418	30	45	0	54.02

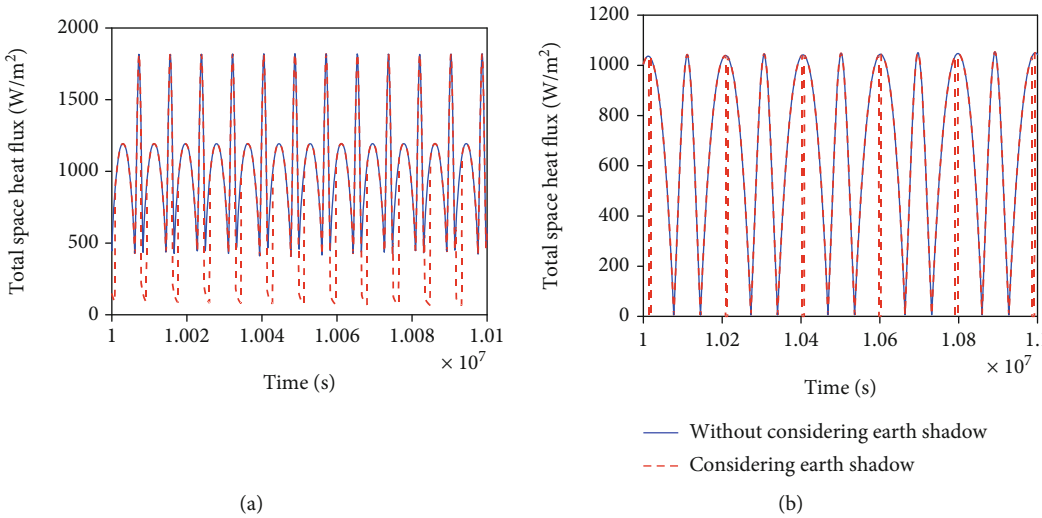

Figure 6: Space heat flux received by the membrane antenna structure: (a) low orbit; (b) high orbit.

coordinate matrix of $\vec{z}$ in the $C_0x_0y_0z_0$ frame, $\mathbf{z}'$ represents the coordinate matrix of vector $\vec{z}$ in the $C_1x_1y_1z_1$ frame, and

$$\tilde{z} = \begin{bmatrix} 0 & -z_3 & z_2 \\ z_3 & 0 & -z_1 \\ -z_2 & z_1 & 0 \end{bmatrix} \tag{31}$$

is the skew symmetric matrix of z.

3.2. Component Synthesis Vibration Suppression Control Design. For flexible spacecraft, attitude maneuver will cause the vibration of the flexible appendage, and the vibration will affect the performance of the spacecraft adversely. The component synthesis vibration suppression (CSVS) method has been widely used in the vibration reduction of flexible spacecraft during attitude maneuver [36, 37]. CSVS is a vibration self-canceled method, by which the vibration excited by the former input can be canceled by other inputs with suitable time delays [38]. Because the CSVS control can be performed without state feedback, therefore it is easy for practical application. Figure 5 demonstrates the simplest example of application of the CSVS method. For a single-degree-of-freedom (SDOF) undamped system, the dynamic equation can be expressed as

$$\ddot{x} + \omega^2 x = F(t), \tag{32}$$

where x is the state coordinate of the system, ω is the natural frequency, $P = 2\pi/\omega$ is the vibration period of the SDOF system, and $F(t)$ is the control input.

Supposing two excitations (impulse 1 and impulse 2) are applied on the SDOF system, it can be seen clearly from Figure 5 that the vibration excited by impulse 1 at time 0 is canceled by impulse 2 implemented at time $P/2$. Ideally, no vibration existed after such superimposition. Based on

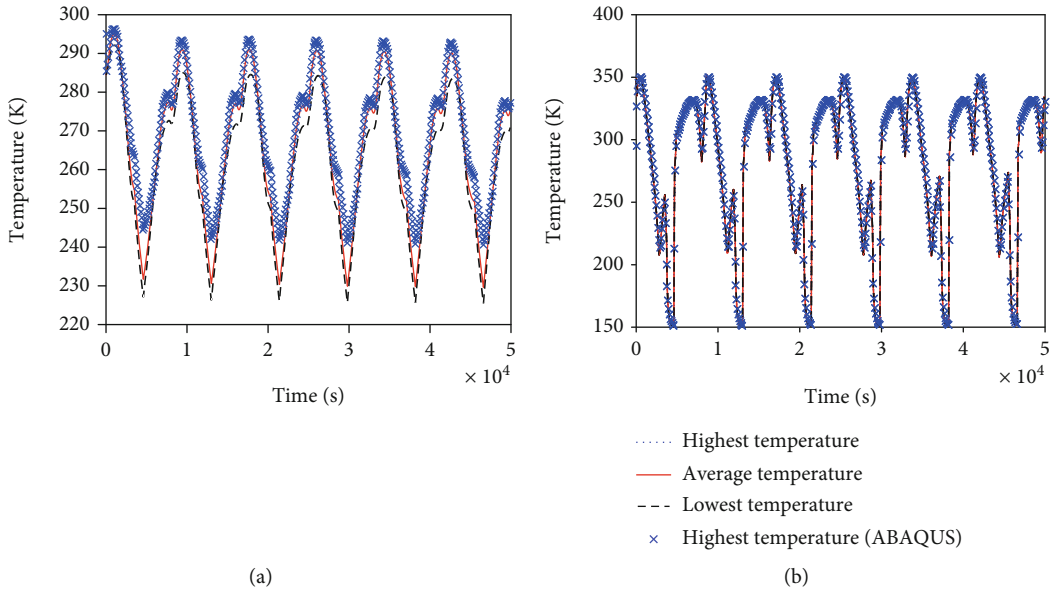

Figure 7: Temperature vs. time graph of the membrane antenna structure in low orbit: (a) support frame; (b) membrane array.

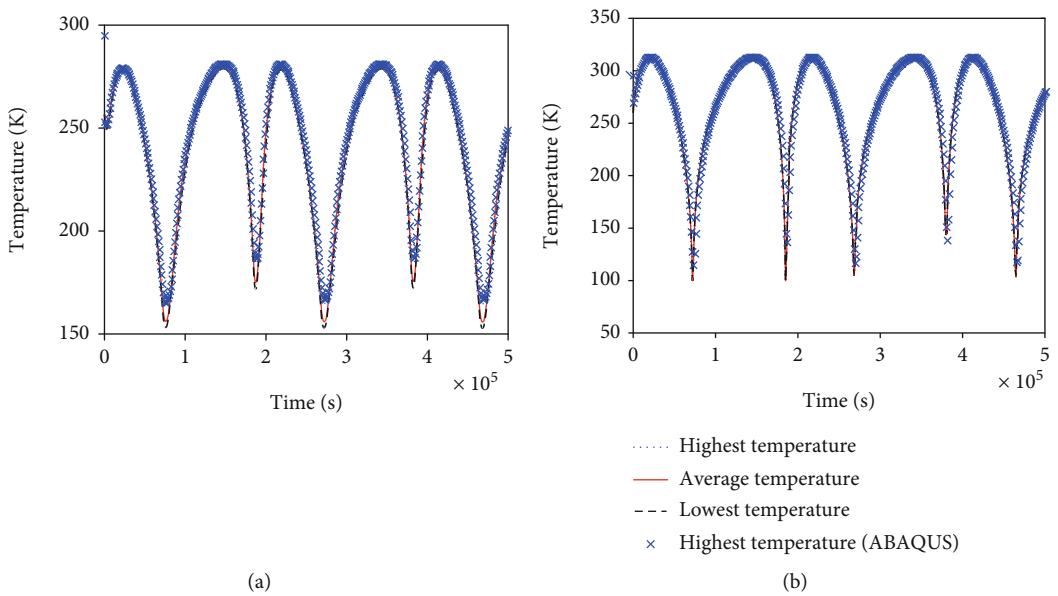

Figure 8: Temperature vs. time graph of the membrane antenna structure in high orbit: (a) support frame; (b) membrane array.

Table 3: Thermal deformation of the membrane antenna structure.

Space heat flux (W/m^2)	Maximum deformation of the support frame (mm)			Maximum deformation of the membrane array (mm)		
	x direction	y direction	z direction	x direction	y direction	z direction
1831 (maximal heat flux in the low orbit)	0.41	0.13	0	20	21	0
1089 (maximal heat flux in the high orbit)	1.25	0.40	0	11	12	0
872.4 (average heat flux in the low orbit)	4.08	1.31	0	5.29	7.84	0
667.2 (average heat flux in the high orbit)	3.81	1.22	0	4.60	7.19	0
56.2 (minimal heat flux in the low orbit)	17	5.58	0	18	14	0
1.04 (minimal heat flux in the high orbit)	35	9.98	0	25	21	0

Table 4: Nature frequencies of the membrane antenna structure under different heat fluxes.

	First-order nature frequency	Second-order nature frequency	Third-order nature frequency	Fourth-order nature frequency	Fifth-order nature frequency	Sixth-order nature frequency
No thermal effect	0.307	0.310	0.674	0.791	0.933	1.086
1831 W/m^2	0.378	0.395	0.934	1.179	1.451	1.671
1089 W/m^2	0.349	0.356	0.810	0.981	1.186	1.404
872.4 W/m^2	0.548	0.548	0.735	0.812	0.926	1.063
56.2 W/m^2	—	—	1.061	1.061	1.414	1.414
1.04 W/m^2	—	1.296	1.296	—	—	2.417

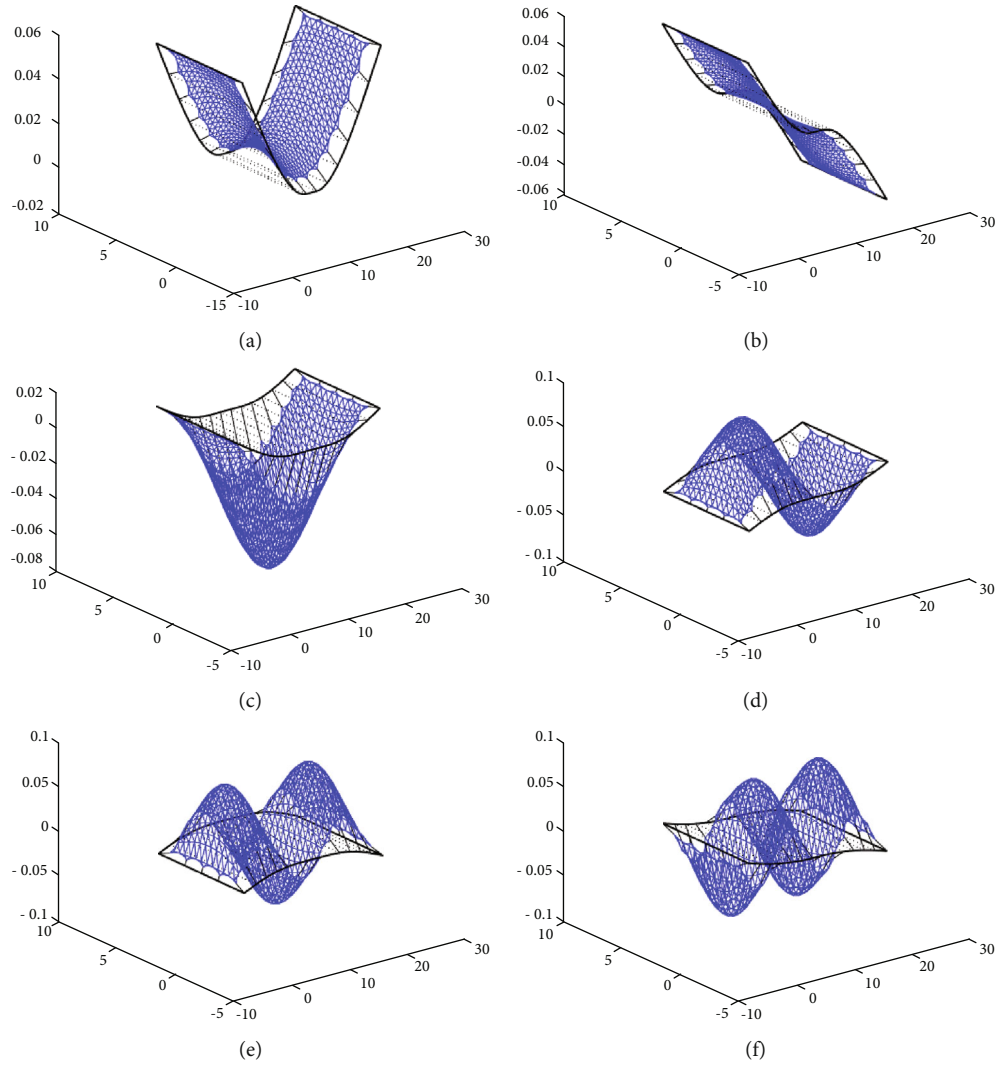

Figure 9: Vibration modes of the membrane antenna structure without considering thermal effects: (a) first mode; (b) second mode; (c) third mode; (d) fourth mode; (e) fifth mode; (f) sixth mode.

this ideal, a CSVS control command can be designed following the theorem below.

Theorem 1 (see [39]). *For a system of equation (32) under zero initial conditions, if the m vibration period is divided into n (m and n are relatively prime) equal parts, and at the beginnings of every equal part or at the points delayed from it by integral multiple periods, one of the n-identical components is applied, then the system will not vibrate when all the commands are out of action.*

It should be noted that "identical components" refer to commands which have the same time-varying characteristics

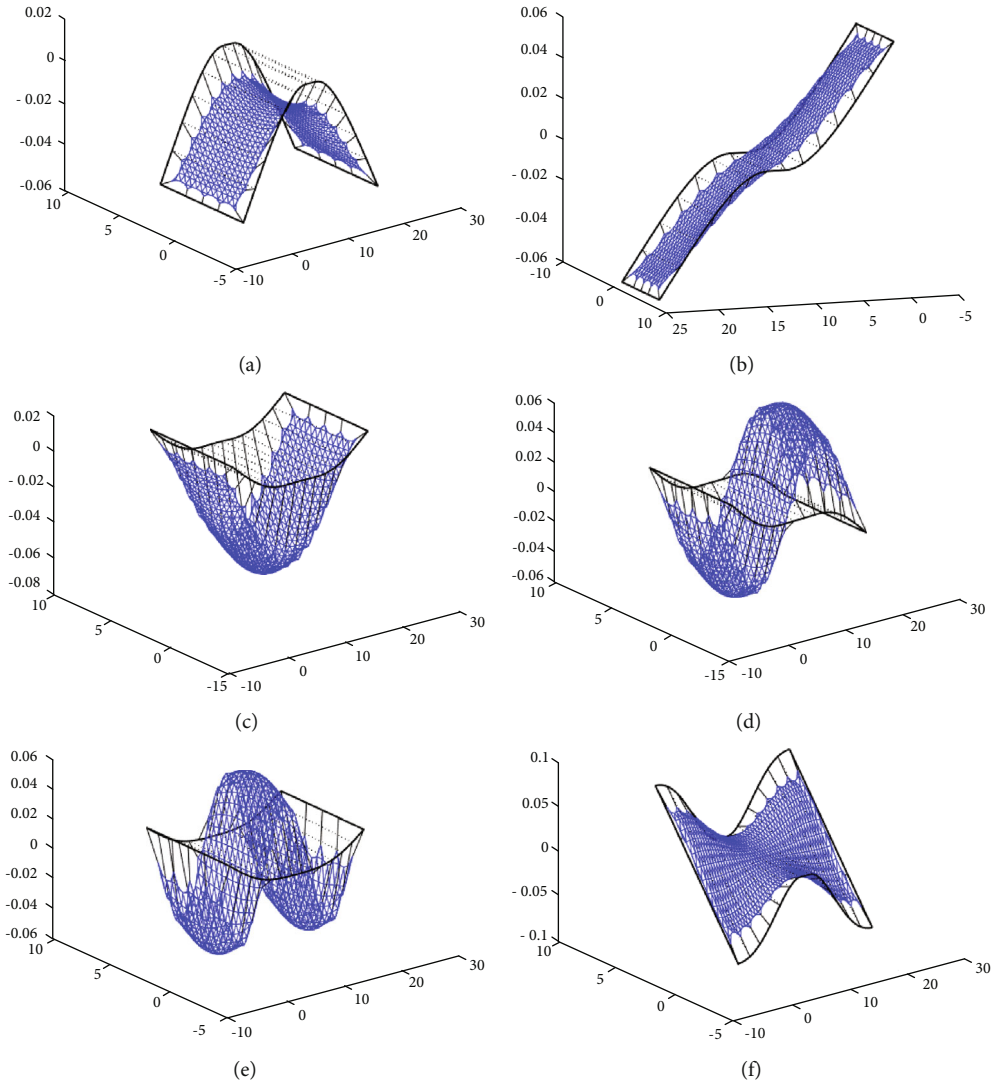

Figure 10: Vibration modes of the membrane antenna structure under the heat flux as 1831 W/m2: (a) first mode; (b) second mode; (c) third mode; (d) fourth mode; (e) fifth mode; (f) sixth mode.

and the same amplitude, and the CSVS method is not only effective for impulse components but also effective for arbitrary number of components in any time-varying function form.

4. Numerical Simulations

The numerical simulation results for the thermal analysis and dynamic study of the satellite with membrane antenna structure are presented and discussed in this section. The mechanical and thermal parameters of the membrane-antenna-satellite system are shown in Table 1.

The thermal analysis is preformed first. The orbital parameters for the membrane antenna are shown in Table 2. Two orbits, denoted as low orbit and high orbit, are studied in our work, as shown in Table 2. Considering the functionality of the space membrane antenna, the antenna structure is supposed to track and catch the Earth all the time. Therefore, the normal of the membrane antenna surface is assumed to be parallel to the Earth vector, and the sun angle is calculated correspondingly based on the orbital position of the spacecraft. The space heat flux received by the membrane antenna structure is calculated and shown in Figure 6. It can be seen clearly from Figure 6 that the space heat flux will vary periodically with the spacecraft orbiting. Generally, the space heat flux of the low orbit is higher than that of the high orbit. And, the space heat flux will change dramatically once the spacecraft goes through an eclipse.

Based on the calculated space heat flux, and by using the proposed finite element thermal model, the temperature field of the membrane antenna structure can be obtained. For comparison, the temperature field of the structure is also calculated by using ABAQUS. The membrane antenna structure is discretized into 3880 elements in ABAQUS, the membrane array is modeled with the S4RT element, and

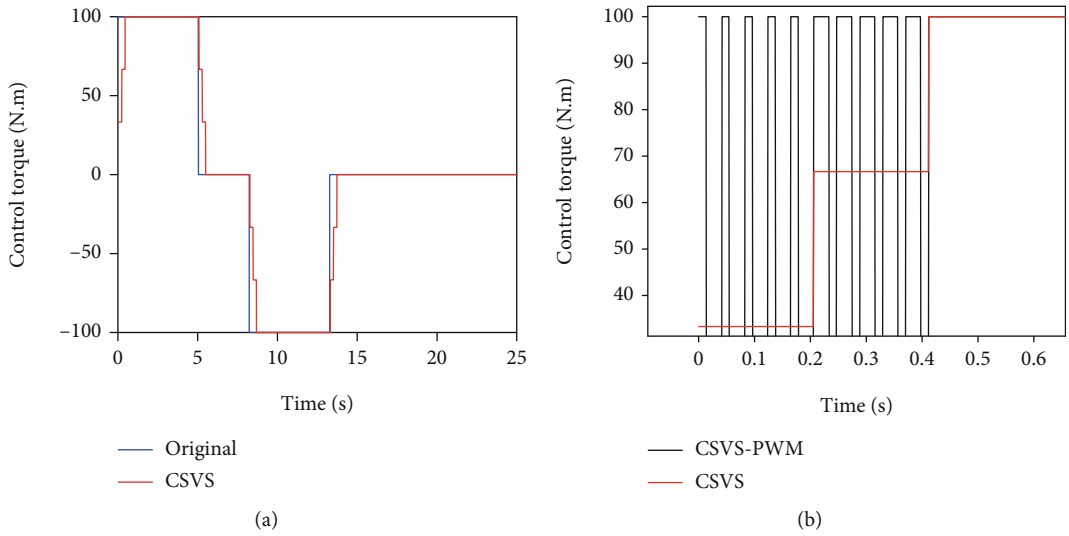

Figure 11: (a) CSVS command with zero-order robust and three components; (b) PWM transfer of CSVS command.

the support frame is modeled with the C3D4T element. Figure 7 shows the temperature of the support frame and membrane array in low orbit. From Figure 7, we can see that the temperature results obtained by the proposed model coincide extremely well with the results obtained by ABAQUS, which shows the correctness of the proposed thermal analysis model. It also can be seen that the temperature will change periodically with the membrane antenna orbiting; the temperature-varying range of the support frame is [225 K, 296 K] and the temperature-varying range of the membrane array is [150 K, 350 K]; at each time instant, the membrane array has an almost uniform temperature field because of the planar configuration. The temperature analysis results for the high-orbit case are shown in Figure 8. We can see that, for the high-orbit case, the temperature results obtained by the proposed model also coincide well with the results of ABAQUS; the temperature-varying range of the support frame is [153 K, 280 K] and the temperature-varying range of the membrane array is [100 K, 312 K]; at each time instant, the membrane array will also have an almost uniform temperature field. From the temperature analysis results, we can see that the membrane antenna structure could have a temperature variation as large as 200 K in orbit. This will induce a considerable thermal deformation to the structure and change the dynamic properties significantly. Table 3 shows the thermal deformation of the membrane antenna structure under different space heat fluxes. It can be seen that the thermal deformation of the membrane antenna structure is nonnegligible especially when the spacecraft is in the Earth's shadow. And the structure will only have an in-plane thermal deformation because of the planar configuration.

Considering the influence of thermal stress caused by the thermal deformation, modal analysis of the membrane antenna structure has been performed herein. Table 4 shows the nature frequencies of the structure under different space heat fluxes. From Table 4, we can see that the nature frequencies of the membrane antenna structure are affected significantly by the thermal environment. We can also see from Table 4 that for low-heat-flux cases (the membrane antenna structure is in the Earth's shadow), some low-order modes will become local modes and even complex modes (represented by "—" in Table 4). The reason of this phenomenon is that for these low-heat-flux cases, the membrane structure cannot hold when stretched because of the large thermal deformation. The mode shapes of the membrane antenna structure are shown in Figures 9 and 10. We can see that the heat flux will also change the mode shapes of the structure by influencing the stress distribution. Therefore, for space membrane structures, to capture the dynamic properties accurately, the thermal analysis must be performed first.

Based on the rigid-flexible coupling dynamic model established in Section 3, the rigid-flexible coupling dynamics of the membrane-antenna-satellite system is studied herein. Assuming the satellite will have a single-axis rest-to-rest maneuver that rotates 30° around the y_1-axis for 25 s, the control command for such a rest-to-rest issue can be obtained by using the time-fuel optimal control method [40], as shown by the blue line in Figure 11(a). Suppose the space heat flux on the membrane antenna structure is 1831 W/m^2 at the initial time, the heat flux and temperature of the membrane antenna structure during the attitude maneuver are calculated and shown in Figure 12. It can be seen from Figure 12 that the heat flux will change obviously with the attitude maneuvering; however, the temperature variation of the structure is limited because the attitude maneuver time is short. Based on the rigid-flexible dynamic model presented in Section 3, the dynamic response of the membrane-antenna-satellite system during the attitude maneuver is calculated and shown in Figure 13. Here, for comparison, the dynamic response of the membrane-antenna-satellite system without considering thermal effects

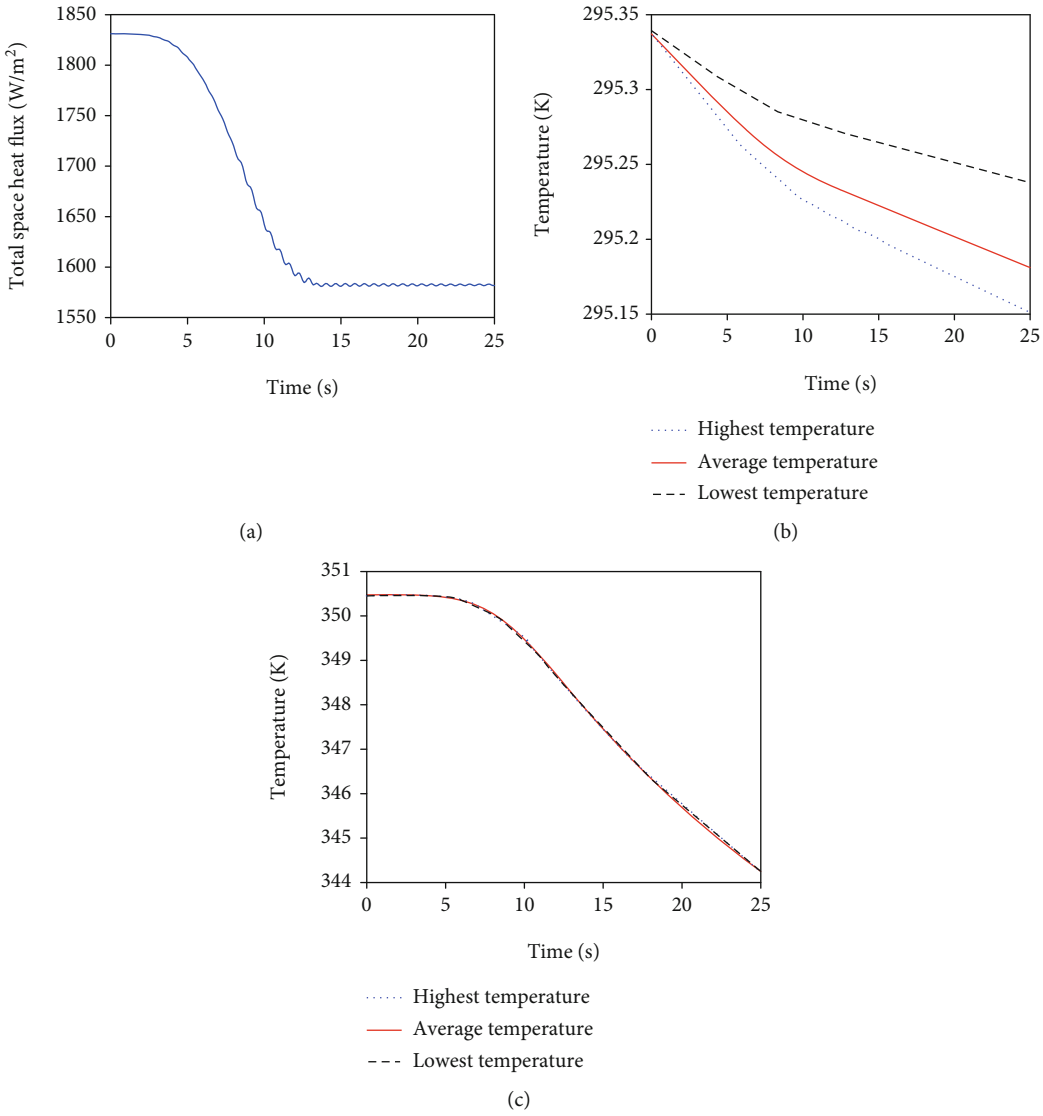

Figure 12: Heat flux and temperature of the membrane antenna structure during attitude maneuver: (a) heat flux absorbed by the structure; (b) temperature of the support frame; (c) temperature of the membrane array.

is also presented, as shown by the blue solid line in Figure 13. We can see from Figure 13 that the rigid-flexible dynamics is affected obviously by the thermal stress induced by the space heat flux. Therefore, to capture the dynamic properties of the satellite-membrane-antenna system precisely, the thermal effects must be considered. From Figure 13, we can also see that, although the system can realize the desired attitude maneuver in general, however, because of the vibration of the membrane antenna structure, the attitude angle and the angular velocity will oscillate significantly. Because the nature frequencies of the membrane antenna structure are increased with the thermal stress considered in this case, as shown in Table 4, the oscillation frequency of the attitude angle and the angular velocity with thermal stress considered will be higher.

To reduce the vibration of the membrane antenna structure caused by the attitude maneuver, the CSVS method has been utilized. The control command obtained by the time-fuel optimal control method is treated as a component, and by arranging the similar components along the time axis according to the rules of CSVS, the control input that can realize the desired attitude maneuver and reduce the vibration of the flexible appendage is constructed and shown as the red line in Figure 11(a). Because the temperature variation of the structure is limited during the attitude maneuver, here, the second-order nature frequency of the membrane antenna structure under heat flux at 1831 W/m^2 is chosen as the target frequency. In practice, the attitude maneuver of a satellite usually relies on the on-off thruster which can only produce constant control torque. So, in this paper, the pulse width modulation (PWM) method has been used to modulate the CSVS control command. Pulse width modulation (PWM) can turn a signal with varying amplitude into a pulse signal with constant amplitude; the width of the pulse

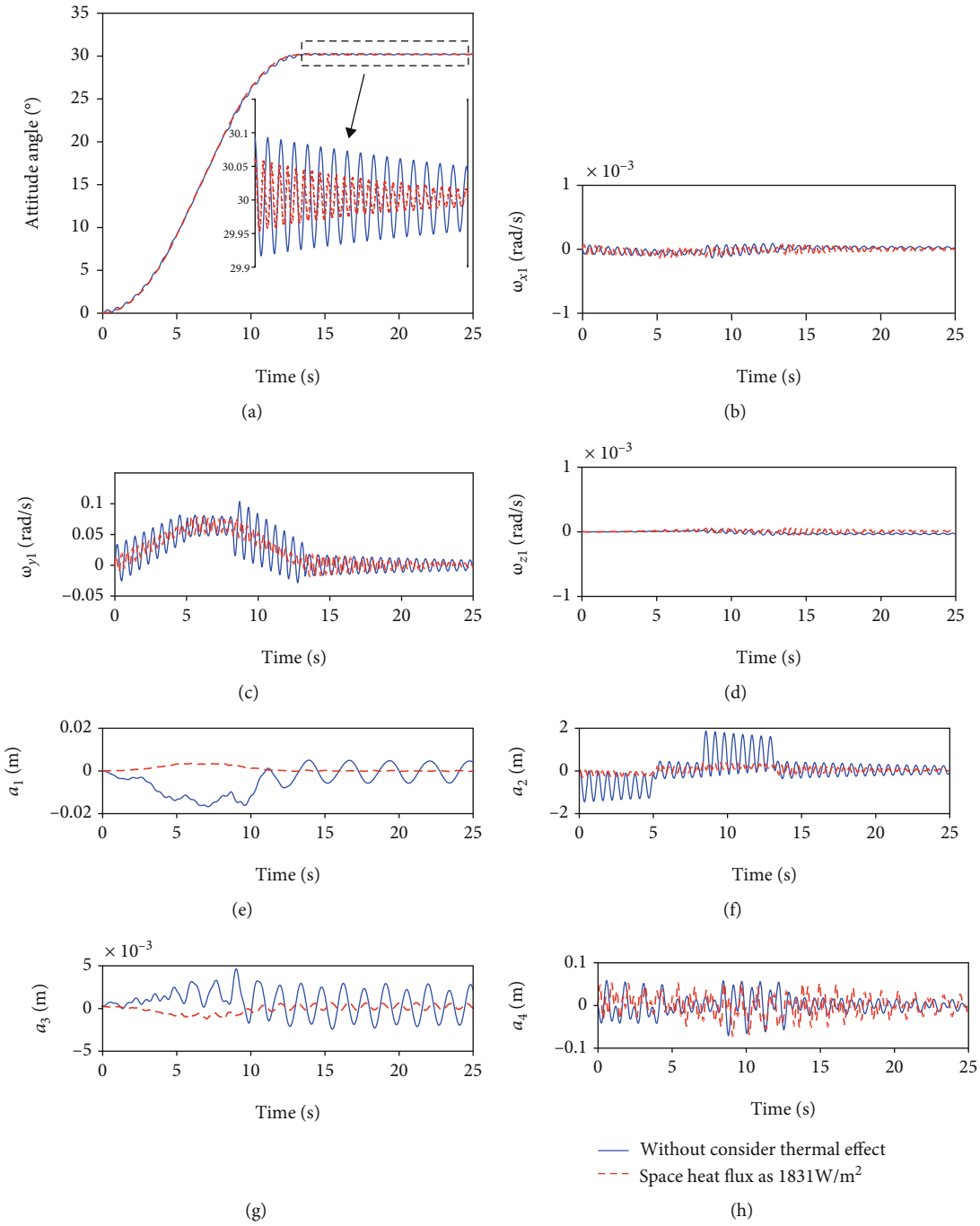

FIGURE 13: Dynamic response of the satellite-membrane-antenna system during the attitude maneuver with and without thermal effects considered: (a) attitude angle; (b) angular velocity in the x_1 direction; (c) angular velocity in the y_1 direction; (d) angular velocity in the z_1 direction; (e) first-order modal coordinate; (f) second-order modal coordinate; (g) third-order modal coordinate; (h) fourth-order modal coordinate.

is proportional to the amplitude of the original signal. By using the PWM, an on-off control command can be obtained for the firing thruster. Figure 11(b) shows the CSVS control command after PWM transformation. With the control command shown in Figure 11(b), control results of the satellite with membrane antenna are obtained and shown in Figure 14. It can be seen clearly that by using the CSVS control method, we can realize the desired attitude maneuver and reduce the vibration of the membrane antenna structure at the same time. From Figure 14, we can also see that with the proposed CSVS controller, the errors of the attitude angle and angular velocity can be kept at a very

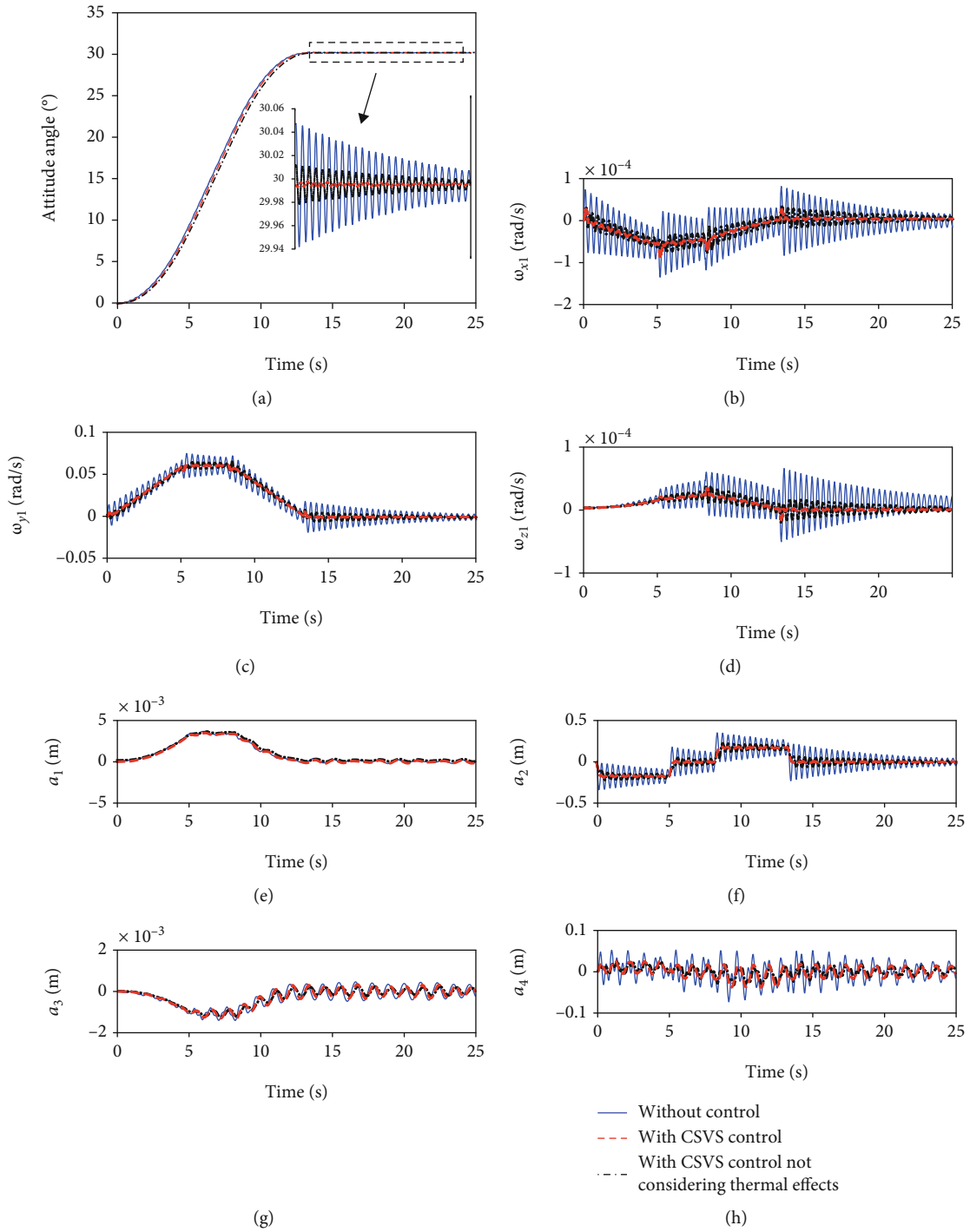

FIGURE 14: Dynamic response of the satellite-membrane-antenna system during the attitude maneuver with CSVS control: (a) attitude angle; (b) angular velocity in the x_1 direction; (c) angular velocity in the y_1 direction; (d) angular velocity in the z_1 direction; (e) first-order modal coordinate; (f) second-order modal coordinate; (g) third-order modal coordinate; (h) fourth-order modal coordinate.

low level, which shows the effectiveness of the presented control method. In Figure 14, the CSVS control results when the thermal effects are not considered have also been shown, represented by the black dash-dot line. Here, the CSVS controller is designed based on the dynamic model of the membrane-antenna-satellite system in which the thermal effects are not considered. We can see that the control effectiveness of the CSVS controller will be improved significantly once the thermal effects are considered.

Due to the inevitable modeling errors, the established theoretical model cannot be exactly equivalent to the actual system, so the robustness of the controller is very important,

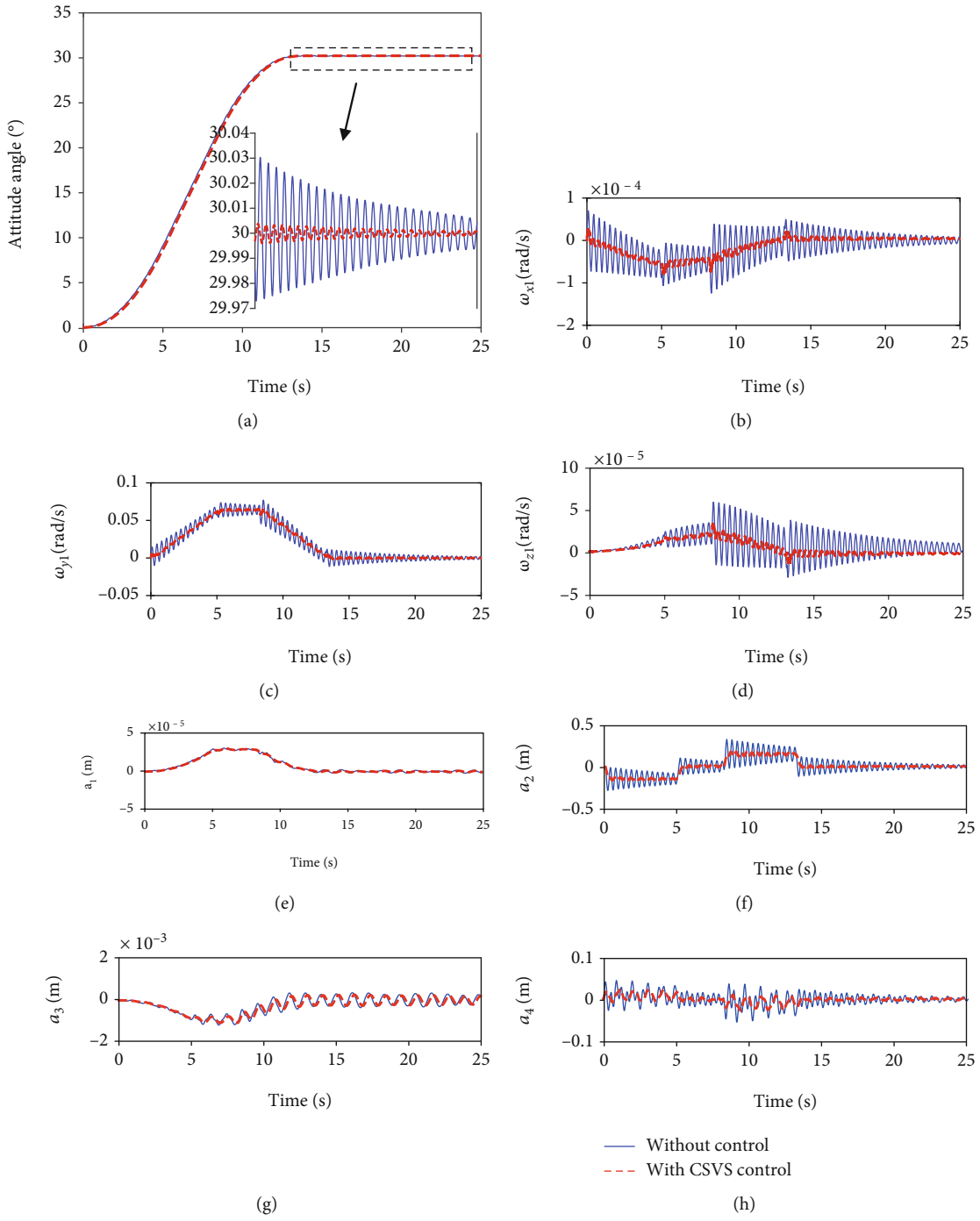

Figure 15: Dynamic response of the satellite-membrane-antenna system during the attitude maneuver with modeling disturbance under CSVS control: (a) attitude angle; (b) angular velocity in the x_1 direction; (c) angular velocity in the y_1 direction; (d) angular velocity in the z_1 direction; (e) first-order modal coordinate; (f) second-order modal coordinate; (g) third-order modal coordinate; (h) fourth-order modal coordinate.

especially for spacecraft. The robustness of the proposed control method with regard to model parameter disturbance is studied numerically here. Suppose the prestress of the membrane antenna structure is 10% higher than the nominal value, the control results are obtained and shown in Figure 15. From Figure 15, we can see that the proposed control method can still control the attitude maneuver accurately while suppressing the vibration effectively in the presence of model parameter disturbance.

5. Conclusion

In this paper, the rigid-flexible coupling dynamics and control of a satellite with membrane antenna considering

thermal effects have been studied. The thermal analysis model of the membrane antenna structure is established based on the finite element method. The temperature field and thermal deformation of the structure are investigated under different space thermal fluxes. The influences of thermal stress on nature frequencies and vibration modes have been unveiled, and then, the rigid-flexible coupling dynamic model of the membrane-antenna-satellite system is established with the thermal stress considered. To reduce the vibration of the membrane antenna structure caused by the attitude maneuver, a controller is designed based on the component synthesis vibration suppression (CSVS) method. The main conclusions drawn from the study can be summarized as follows:

(1) The thermal flux received by the membrane antenna structure will change periodically with the spacecraft orbiting. The temperature variation of the membrane antenna structure can be as large as 200 K in orbit

(2) The dynamic properties of the membrane antenna structure are affected significantly by the thermal stress, especially when the spacecraft is in an eclipse

(3) The thermal effects have an nonnegligible influence on the rigid-flexible coupling dynamics of the membrane-antenna-satellite system. The presented CSVS controller can fulfil the desired attitude maneuver meanwhile suppressing the vibration of the membrane antenna structure effectively.

The research outcomes of this paper can provide some reference to the dynamic modeling and control of membrane spacecraft.

Appendix

Vibration Modes of the Membrane Antenna Structure considering the Thermal Effects

Figure 9 shows the first-six vibration modes of the membrane structure without considering thermal effects. It can be seen that the low-order vibration modes are all out-of-plane bending modes. These modes will interact with the attitude motion of the satellite and affect the normal functioning of the membrane antenna. Figure 10 shows the first-six vibration modes of the membrane structure when the space heat flux is 1831 W/m^2. By comparing Figures 9 and 10, we can see that the mode shapes will also change once the thermal stress is considered.

Data Availability

The data used to support the findings of this study are available from the corresponding author upon request.

Conflicts of Interest

The authors declare that they have no conflict of interest.

Acknowledgments

This work was supported by the National Natural Science Foundation of China (grant numbers 12102252 and 12172214) and China Postdoctoral Science Foundation (grant number 2021M692070).

References

[1] T. Liu, X. H. Wang, X. M. Qiu, and X. Zhang, "Theoretical study on the parameter sensitivity over the mechanical states of inflatable membrane antenna," *Aerospace Science and Technology*, vol. 102, article 105843, 2020.

[2] G. Rait and D. Beasley, "Large area membrane apertures for space applications, fabrication and mechanical testing," in *4th AIAA Spacecraft Structures Conference*, Grapevine, Texas, January 2017.

[3] C. Liu and Y. Shi, "Comprehensive structural analysis and optimization of the electrostatic forming membrane reflector deployable antenna," *Aerospace Science and Technology*, vol. 53, pp. 267–279, 2016.

[4] R. Xu, D. X. Li, J. P. Jiang, and W. Liu, "Nonlinear vibration analysis of membrane SAR antenna structure adopting a vector form intrinsic finite element," *Journal of Mechanics*, vol. 31, no. 3, pp. 269–277, 2015.

[5] V. J. Modi, "Attitude dynamics of satellites with flexible appendages - a brief review," *Journal of Spacecraft and Rockets*, vol. 11, no. 11, pp. 743–751, 1974.

[6] X. Liu, L. L. Lv, and G. P. Cai, "Hybrid control of a satellite with membrane antenna considering nonlinear vibration," *Aerospace Science and Technology*, vol. 117, article 106962, 2021.

[7] J. D. Johnston and E. A. Thornton, "An evaluation of thermally-induced structural disturbances of spacecraft solar arrays," in *IECEC 96. Proceedings of the 31st Intersociety Energy Conversion Engineering Conference*, Washington DC, USA, August 1996.

[8] E. A. Thornton, G. P. Chini, and D. W. Gulik, "Thermally induced vibrations of a self-shadowed split-blanket solar array," *Journal of Spacecraft and Rockets*, vol. 32, no. 2, pp. 302–311, 1995.

[9] G. Y. Lu, J. Y. Zhou, G. P. Cai, G. Q. Fang, L. L. Lv, and F. J. Peng, "Studies of thermal deformation and shape control of a space planar phased array antenna," *Aerospace Science and Technology*, vol. 93, article 105311, 2019.

[10] M. Amabili, *Nonlinear Vibrations and Stability of Shells and Plates*, Cambridge University Press, Cambridge, 2008.

[11] X. Liu, G. P. Cai, F. J. Peng, H. Zhang, and L. L. Lv, "Nonlinear vibration analysis of a membrane based on large deflection theory," *Journal of Vibration and Control*, vol. 24, no. 12, pp. 2418–2429, 2018.

[12] J. Li and S. Yan, "Thermally induced vibration of composite solar array with honeycomb panels in low earth orbit," *Applied Thermal Engineering*, vol. 71, no. 1, pp. 419–432, 2014.

[13] L. Liu, D. Cao, H. Huang, C. Shao, and Y. Xu, "Thermal-structural analysis for an attitude maneuvering flexible spacecraft under solar radiation," *International Journal of Mechanical Sciences*, vol. 126, pp. 161–170, 2017.

[14] J. Liu and K. Pan, "Rigid-flexible-thermal coupling dynamic formulation for satellite and plate multibody system," *Aerospace Science and Technology*, vol. 52, pp. 102–114, 2016.

[15] Q. Hu and G. Ma, "Variable structure control and active vibration suppression of flexible spacecraft during attitude maneuver," *Aerospace Science and Technology*, vol. 9, no. 4, pp. 307–317, 2005.

[16] Q. Hu, P. Shi, and H. Gao, "Adaptive variable structure and commanding shaped vibration control of flexible spacecraft," *Journal of Guidance, Control, and Dynamics*, vol. 30, no. 3, pp. 804–815, 2007.

[17] L. Liu, D. Q. Cao, and J. Wei, "Rigid-flexible coupling dynamic modeling and vibration control for flexible spacecraft based on its global analytical modes," *Science China Technological Sciences*, vol. 62, no. 4, pp. 608–618, 2019.

[18] Y. T. Cao, D. Q. Cao, G. Q. He, and L. Liu, "Thermal alternation induced vibration analysis of spacecraft with lateral solar arrays in orbit," *Applied Mathematical Modelling*, vol. 86, pp. 166–184, 2020.

[19] Y. Q. Cui, P. Lan, H. T. Zhou, and Z. Yu, "The rigid-flexible-thermal coupled analysis for spacecraft carrying large-aperture paraboloid antenna," *Journal of Computational and Nonlinear Dynamics*, vol. 15, no. 3, article 031003, 2020.

[20] M. Shahravi and M. Azimi, "Attitude and vibration control of flexible spacecraft using singular perturbation approach," *International Scholarly Research Notices*, vol. 2014, Article ID 163870, 13 pages, 2014.

[21] M. Shahravi and M. Azimi, "A comparative study for collocated and non-collocated sensor/actuator placement in vibration control of a maneuvering flexible satellite," *Proceedings Of The Institution Of Mechanical Engineers, Part C: Journal Of Mechanical Engineering Science*, vol. 229, no. 8, pp. 1415–1424, 2015.

[22] M. Azimi and M. Shahravi, "Stabilization of a large flexible spacecraft using robust adaptive sliding hypersurface and finite element approach," *International Journal of Dynamics and Control*, vol. 8, no. 2, pp. 644–655, 2020.

[23] M. Azimi and E. F. Joubaneh, "Dynamic modeling and vibration control of a coupled rigid-flexible high-order structural system: a comparative study," *Aerospace Science and Technology*, vol. 102, article 105875, 2020.

[24] Y. Liu, X. Li, Y. J. Qian, and H. L. Yang, "Rigid-flexible coupled dynamic and control for thermally induced vibration and attitude motion of a spacecraft with hoop-truss antenna," *Applied Sciences*, vol. 12, no. 3, p. 1071, 2022.

[25] Y. Shen, W. Zheng, and X. Wang, "Dynamic and vibration analysis of a SAR membrane antenna," in *Proceedings of ASMEInternational Mechanical Engineering Congress and Exposition*, Washington, USA, Novemver 2007.

[26] H. Fang, B. Yang, H. Ding, J. Hah, U. Quijano, and J. Huang, "Dynamic analysis of large in-space deployable membrane antennas," 2006.

[27] X. Liu, G. P. Cai, F. J. Peng, and H. Zhang, "Dynamic model and active vibration control of a membrane antenna structure," *Journal of Vibration and Control*, vol. 24, no. 18, pp. 4282–4296, 2018.

[28] X. Liu, H. Zhang, L. L. Lv, F. Peng, and G. Cai, "Vibration control of a membrane antenna structure using cable actuators," *Journal of the Franklin Institute*, vol. 355, no. 5, pp. 2424–2435, 2018.

[29] J. Li, S. Yan, and R. Cai, "Thermal analysis of composite solar array subjected to space heat flux," *Aerospace Science and Technology*, vol. 27, no. 1, pp. 84–94, 2013.

[30] J. A. Foster and G. S. Aglietti, "The thermal environment encountered in space by a multifunctional solar array," *Aerospace Science and Technology*, vol. 14, no. 3, pp. 213–219, 2010.

[31] R. Nneill and J. Zich, "Space structure heating/SSQ/a numerical procedure for analysis of shadowed space heating of sparse structures," in *16th Thermophysics Conference*, June 1981Palo Alto, California, June.

[32] M. E. Brown, *Introduction to Thermal Analysis: Techniques and Applications*, Springer Science & Business Media, Berlin, 2001.

[33] J. N. Reddy, *An Introduction to the Finite Element Method*, McGraw-Hill, New York, 2019.

[34] E. M. Sparrow and E. R. Niewerth, "Radiating, convecting and conducting fins: numerical and linearized solutions," *International Journal of Heat and Mass Transfer*, vol. 11, no. 2, pp. 377–379, 1968.

[35] A. M. Browder and R. M. Alexander, "A general approach to modal analysis for time-varying systems," in *29th Structures, Structural Dynamics and Materials Conference*, Williamsburg, VA, April 1988.

[36] L. Zhang, S. J. Xu, Z. P. Zhang, and N. Cui, "Active vibration suppression for flexible satellites using a novel component synthesis method," *Advances in Space Research*, vol. 67, no. 6, pp. 1968–1980, 2021.

[37] L. Zhang, S. Xu, X. Ju, and N. Cui, "Flexible satellite control via fixed-time prescribed performance control and fully adaptive component synthesis vibration suppression," *Nonlinear Dynamics*, vol. 100, no. 4, pp. 3413–3432, 2020.

[38] J. J. Shan and D. Liu, "Study on component synthesis active vibration suppression method for flexible structures," *Aerospace Shanghai*, vol. 6, pp. 28–37, 2001.

[39] J. Y. Zhang, T. Liu, and Z. P. Zhang, "Study on component synthesis active vibration suppression method using zero-placement technique," *Chinese Journal of Aeronautics*, vol. 21, no. 4, pp. 304–312, 2008.

[40] S. W. Liu and T. Singh, "Fuel/time optimal control of spacecraft maneuvers," *Journal of Guidance, Control, and Dynamics*, vol. 20, no. 2, pp. 394–397, 1997.